BASIC RESEARCH PAPER

Autophagy 10:10, 1738–1748; October 2014; © 2014 Landes Bioscience

The nascent polypeptide-associated complex is essential for autophagic flux

Bin Guo,[2,†] Jie Huang,[1,2,†] Wenxian Wu,[3] Du Feng,[3] Xiaochen Wang,[4] Yingyu Chen,[1,*] and Hong Zhang[2,*]

[1]Key Laboratory of Medical Immunology; Ministry of Health; Peking University Health Science Center; Beijing, China; [2]State Key Laboratory of Biomacromolecules; Institute of Biophysics; Chinese Academy of Sciences; Beijing, China; [3]Institute of Neurology; Key Laboratory of Age-Associated Cardiac-Cerebral Vascular Disease of Guangdong Province; Affiliated Hospital of Guangdong Medical College; Zhanjiang, China; [4] National Institute of Biological Sciences; Beijing, China

[†]These authors contributed equally to this work.

Keywords: NAC, autophagy, lysosome, *C. elegans*

Abbreviations: *ATG*, autophagy-related (gene); DAPI, 4,6-diamino-2-phenyl indole; EGFR, epidermal growth factor receptor; *epg*, ectopic PGL granules; GFP, green fluorescent protein; ICD, inhibitor of cell death; NAC, nascent polypeptide-associated complex; *NACA*, nascent polypeptide-associated complex alpha subunit; *BTF3*, basic transcription factor 3; ssGFP, signal sequence-GFP fusion protein; SQSTM1, sequestosome 1; CTSB, cathepsin B; CTSD, cathepsin D

The ribosome-associated nascent polypeptide-associated complex (NAC) is involved in multiple cotranslational processes, including protein transport into the ER and mitochondria, and also acts as a chaperone to assist protein folding. Here we demonstrated that NAC is also essential for autophagic degradation of a variety of protein aggregates in *C. elegans*. Loss of function of NAC impairs lysosome function, resulting in accumulation of autophagic substrates in enlarged autolysosomes. Knockdown of mammalian NAC also causes accumulation of nondegradative autolysosomes. Our study revealed that NAC plays an evolutionarily conserved role in the autophagy pathway and thus in maintaining protein homeostasis under physiological conditions.

Introduction

The heterodimeric nascent polypeptide associated complex (NAC), consisting of NACA/α and BTF3/β NAC subunits, associates with the ribosome and is the first cytosolic factor that contacts the nascent polypeptide chain emerging from the ribosome in eukaryotes.[1] NAC shields the growing nascent chain from binding to inappropriate cytosolic factors and thus functions in multiple cotranslational processes.[2,3] NAC contributes to the fidelity of cotranslational targeting of polypeptides to the endoplasmic reticulum (ER) by modulating the specificity and fidelity of the interaction of the signal recognition particle with nascent chains and also the interaction of ribosome nascent chain complexes with the ER membrane.[2,4] NAC plays a role in the attachment of cytosolic ribosomes to mitochondria and promotes cotranslational delivery of proteins into mitochondria.[5,6] NAC also acts as a ribosome-associated chaperone to assist folding of nascent polypeptides and regulates ribosomal function.[7,8] In yeast, simultaneous loss of NAC in the cells depleted for the ribosome-associated chaperone Hsp70-Hsp40 system SSB results in an increase in misfolded protein stress and enhances aggregation of ribosomal proteins and biogenesis factors.[7] The essential function of NAC during multicellular organism development is implicated by the observations that loss of function of NAC causes severe morphological defects, resulting in embryonic lethality in mice, fly, and *C. elegans*.[1,9,10] Loss of NAC activity in *C. elegans* induces misfolded protein stress in the ER, triggering the unfolded protein response (UPR).[11] In response to perturbations of cellular proteostasis, NAC disassociates from ribosomes and redistributes to protein aggregates, resulting in the reduction of translation.[12] However, the mechanisms by which NAC maintains protein homeostasis remain poorly understood.

Macroautophagy (hereafter referred to as autophagy) is a lysosome-mediated degradation process, involving the engulfment of a portion of the cytosolic contents in a double-membrane structure, called the autophagosome, and subsequent delivery of the cargo to the lysosome for degradation.[13,14] In higher eukaryotes, nascent autophagosomes undergo a maturation process by fusing with endosomes to generate hybrid organelles called amphisomes that eventually fuse with lysosomes to produce degradative autolysosomes.[15] Several factors involved in the endolysosomal pathway have been shown to be essential for the maturation of autophagosomes into degradative autolysosomes. For example, impairment of the multisubunit ESCRT complex, which is involved in endocytic sorting of ubiquitinated membrane proteins into multivesicular bodies and their subsequent degradation

*Correspondence to: Yingyu Chen; Email: yingyu_chen@bjmu.edu.cn; Hong Zhang; Email: hongzhang@sun5.ibp.ac.cn
Submitted: 01/13/2014; Revised: 06/13/2014; Accepted: 06/18/2014; Published Online: 07/18/2014
http://dx.doi.org/10.4161/auto.29638

by lysosomes, inhibits autophagosome maturation and causes accumulation of nondegradative autophagic vacuoles.[16,17]

During *C. elegans* embryogenesis, autophagy selectively removes a variety of protein aggregates, including the *C. elegans* SQSTM1/p62 ortholog SQST-1.[18,19] SQST-1 is diffusely localized and weakly expressed in wild-type embryos, while in autophagy mutants it is present at dramatically increased levels and accumulates into a large number of aggregates.[20] Genetic screens for viable mutants with defective degradation of autophagic substrates revealed that the *C. elegans* autophagy machinery contains conserved yeast Atg proteins, highly divergent Atg components, and also metazoan-specific autophagy genes.[19,21-24] Autophagy genes whose loss of function causes pleiotropic effects such as embryonic lethality, however, may fail to be isolated from such genetic screens. In this study, we showed that RNAi inactivation of autophagy genes leads to accumulation of SQST-1 aggregates in larval intestine cells, establishing a genetic model to isolate autophagy genes essential for embryogenesis. From a genome-wide RNAi screen, we found that knockdown of components of NAC results in dramatic accumulation of SQST-1 aggregates in *C. elegans*. NAC is also required for autophagic flux in mammalian cells. We further demonstrated that loss of function of NAC impairs autophagic flux by disrupting lysosome function in *C. elegans* and mammalian cells. Our study revealed an essential function of NAC in autophagy in metazoans.

Results

Genome-wide RNAi screen to identify essential autophagy genes

In *C. elegans*, feeding animals with bacteria expressing dsRNA allows the corresponding gene to be inactivated at specific developmental stages and also modulates the efficacy of gene inactivation. Forward genetic screens isolated a variety of viable autophagy mutants that showed accumulation of SQST-1 aggregates during embryogenesis.[20,25] Unlike genetic mutants, RNAi inactivation of most known autophagy genes, including *epg-1*, *atg-7,* and *atg-2*, failed to cause strong accumulation of SQST-1 aggregates in embryos, suggesting that these autophagy proteins are still present at sufficient levels to mediate autophagic degradation of SQST-1 (data not shown). RNAi inactivation of all autophagy genes, including *vps-34*, *lgg-1*, *bec-1*, *atg-7,* and *epg-5*, however, caused accumulation of a large number of small spherical SQST-1 aggregates in intestinal cells in larvae and adult animals (**Fig. 1A–F**; **Fig. S1A–S1D**). Immunostaining with anti-SQST-1 indicated that in animals with RNAi inactivation of autophagy genes, endogenous SQST-1 accumulated into aggregates in larval intestinal cells (**Fig. S1E–S1J**), and levels of SQST-1 were dramatically increased in an immunoblotting assay (**Fig. 1G**).

We performed a genome-wide RNAi screen to identify genes essential for autophagic removal of SQST-1::GFP at larval stages. Small spherical SQST-1::GFP aggregates accumulated in the intestine in animals with RNAi knockdown of previously identified autophagy genes, and also of genes that are essential for autophagy in other organisms, including *rab-7*, *cdc-48.3* (mammalian *VCP/p97* ortholog), *trpp-8/F46F11.9* (yeast *TRS85* ortholog), and subunits of PP2A.[26-31] Genetic null mutants in these functionally conserved genes are lethal, consistent with the fact that mutations in them have not been identified in previous genetic screens.

Knockdown of *icd-2* and *icd-1* causes defective degradation of SQST-1 and LGG-1

RNAi inactivation of *icd-2* and *icd-1,* which encode the α and β subunits of the nascent polypeptide associated complex (NAC), respectively, caused accumulation of SQST-1::GFP aggregates in the intestine and also in muscle cells (**Fig. 1I–M**; **Fig. S1M–S1P**). Endogenous SQST-1 also formed aggregates and levels of SQST-1 dramatically increased in *icd-2* and *icd-1* knockdown animals (**Fig. 1H**; **Fig. S1K and S1L**). The putative genetic null mutants, *icd-2(tm3125)* and *icd-1(tm2873),* are lethal. Homozygous *icd-2* and *icd-1* mutant animals, derived from *tm3125*/+ and *tm2873*/+ heterozygous mutants, grew into larvae and showed accumulation of SQST-1 aggregates at larval stages (**Fig. S1Q, S1R, S1W, and S1X**). The defect was rescued by a transgene expressing *icd-2* or *icd-1* (**Fig. S1S, S1T, S1Y, and S1Z**). Accumulation of SQST-1 aggregates in *icd-2(RNAi)* and *icd-1(RNAi)* animals was not affected by simultaneous inactivation of the *C. elegans* mTOR ortholog *let-363* (Fig. S1A2–S1F2), suggesting that accumulation of SQST-1 in *icd-2* and *icd-1* mutants could not be suppressed by elevated autophagy activity.

The autophagy protein Atg8 is conjugated to phosphatidylethanolamine that associates with both the outer and inner membrane of the phagophore. Following autophagosome maturation, Atg8 on the outer membrane is cleaved off, while Atg8 on the inner membrane is delivered into the lysosome for degradation. Knockdown of *icd-2* and *icd-1* dramatically increased levels of the lipidated form of the *C. elegans* Atg8 ortholog LGG-1 and also caused the accumulation of LGG-1 puncta in intestinal cells and muscle cells (**Fig. 1H**; **Fig. S2A–S2D**). LGG-1 puncta colocalized with SQST-1 aggregates in *icd-2* and *icd-1* mutant animals (**Fig. 1N–P**). These results suggested that knockdown of components of NAC causes defective autophagic degradation of SQST-1 and LGG-1.

In mutants for autophagy genes acting at early steps of autophagosome formation, including *atg-3*, *atg-7,* and *epg-8*, SQST-1 aggregates were separable from puncta labeled by the lysosomal marker NUC-1::mCherry in the intestine (**Fig. S2E–S2H** and data not shown). However, we found that SQST-1 aggregates and LGG-1 puncta in *icd-2* or *icd-1* mutant animals colocalized with NUC-1::mCherry in intestinal and muscle cells (**Fig. 1Q–X**; **Fig. S2I–S2T**), indicating that SQST-1 aggregates and LGG-1 puncta accumulate in lysosomes. Simultaneous depletion of *atg-3* resulted in SQST-1 aggregates separable from NUC-1-labeled lysosomes in *icd-2* mutants (**Fig. 1Y**–B2).

Loss of function of *icd-2* or *icd-1* impairs lysosomal function

We noticed that loss of function of *icd-2* and *icd-1* affects lysosome morphology. In wild-type animals, lysosomes exhibit distinct tubular and spherical structures in hypodermal and intestinal cells (**Fig. 2A and B**; **Fig. S3A, S3B, S3E, and S3F**;

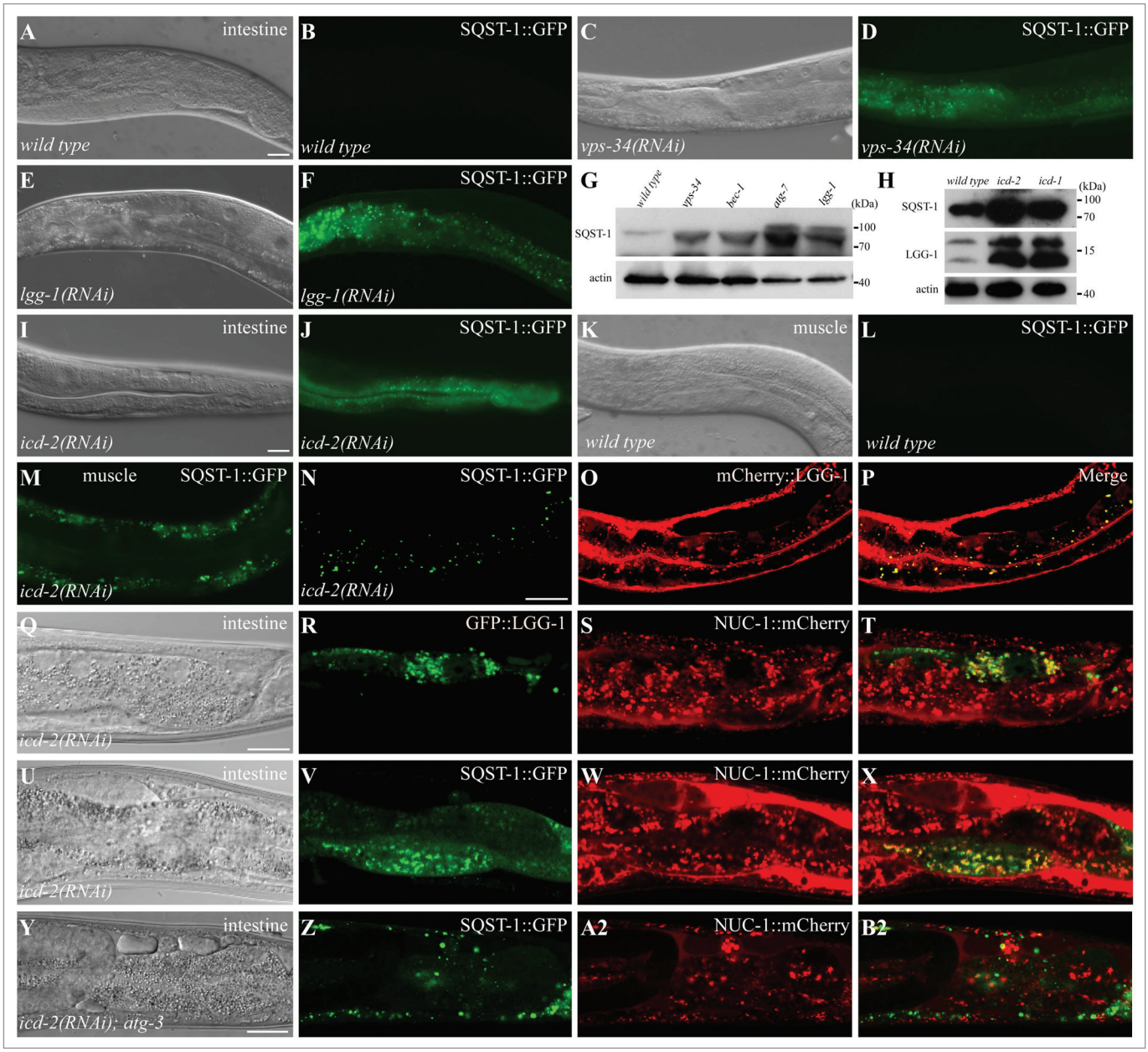

Figure 1. RNAi inactivation of components of the NAC complex causes the accumulation of SQST-1 aggregates. (**A and B**) SQST-1::GFP is weakly expressed and diffusely localized in the intestine in wild-type animals. (**C–F**) SQST-1::GFP accumulates into a large number of small spherical aggregates in the intestine in *vps-34(RNAi)* (**C and D**) and *lgg-1(RNAi)* (**E and F**) animals. (**G**) Compared with wild-type animals, levels of SQST-1 are dramatically elevated in animals with RNAi inactivation of essential autophagy genes in an immunoblotting assay. (**H**) Compared with wild-type animals, levels of SQST-1 and LGG-1 are increased in *icd-2(RNAi)* and *icd-1(RNAi)* animals. (**I and J**) A large number of SQST-1::GFP aggregates accumulate in the intestine in *icd-2(RNAi)* animals. (**K and L**) SQST-1::GFP is weakly expressed and diffusely localized in muscle cells in wild-type animals. (**M**) SQST-1::GFP forms a large number of aggregates in muscle cells in *icd-2(RNAi)* animals. (**A, C, E, I, and K**): Nomarski images of the animals shown in (**B, D, F, J, and L**), respectively. (**N–P**) SQST-1::GFP aggregates colocalize with mCherry::LGG-1 puncta in the intestine in *icd-2(RNAi)* animals. (**Q–X**) GFP::LGG-1 puncta (**Q–T**) and SQST-1::GFP aggregates (**U–X**) in the intestine colocalize with NUC-1::mCherry in *icd-2(RNAi)* animals. (**Y–B2**) SQST-1::GFP aggregates in the intestine are separable from NUC-1::mCherry labeled lysosomes in *icd-2(RNAi); atg-3* double mutants. (**Q, U, and Y**): Nomarski images of the animals shown in the same row. Scale bars (**A–F, I–L, N–P, Q –X, and Y–B2**): 20 μm. Young adult animals were examined.

and data not shown). In *icd-2* or *icd-1* mutant animals, the tubular lysosomes almost disappeared and enlarged spherical lysosomes accumulated instead (**Fig. 2C and D**; **Fig. S3C, S3D, S3G, and S3H**). Enlarged lysosomes labeled by various lysosomal markers, including reporters for LAAT-1 (lysosomal lysine/arginine transporter), NUC-1 (a DNase II ortholog) and LMP-1 (ortholog of mammalian lysosome-associated membrane protein CD68),[32] also accumulated in other cells, including muscle cells and 6 macrophage-like scavenger cells in the body cavity, known as coelomocytes (**Fig. 2E–N and S**). The basal

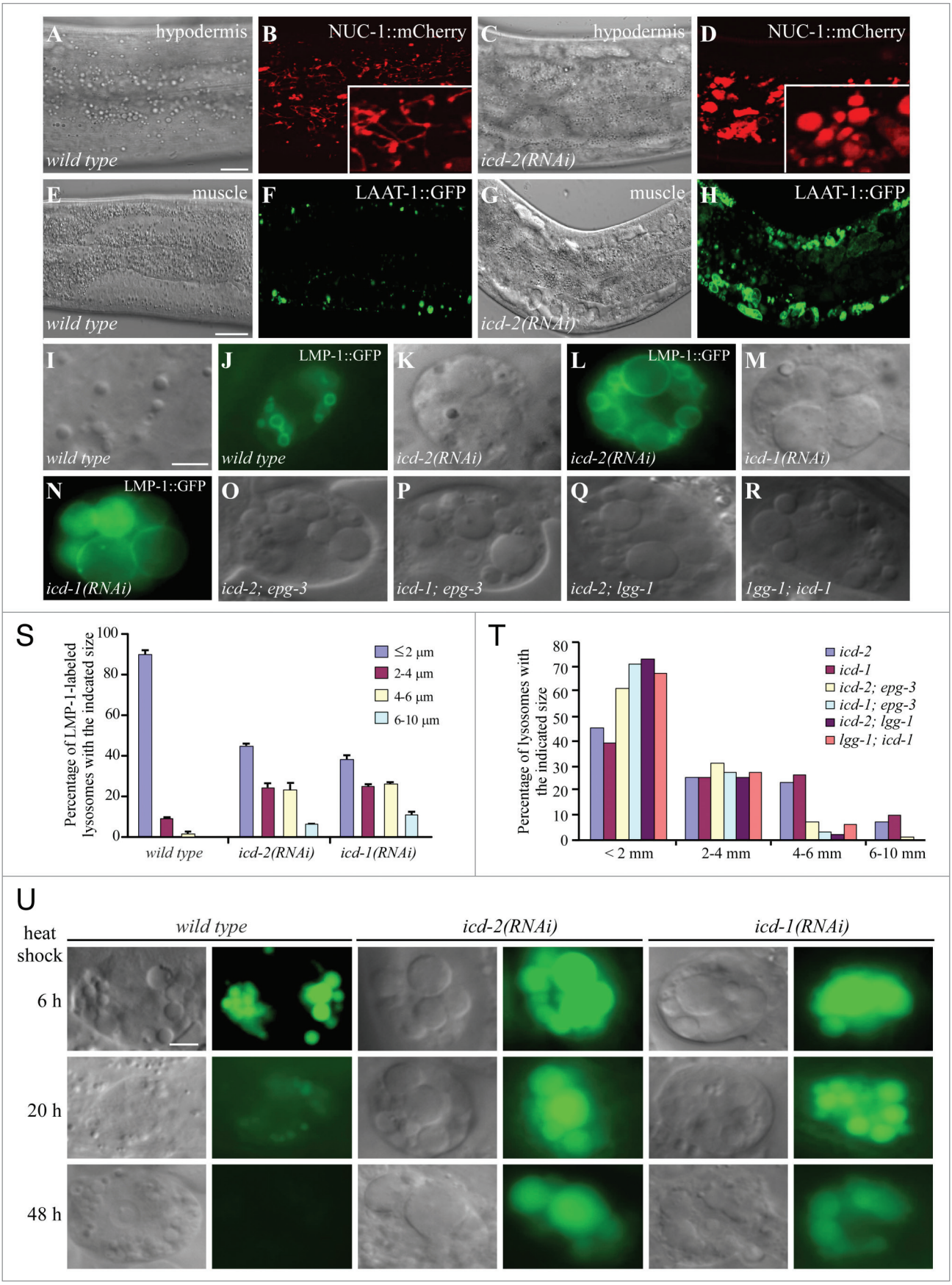

Figure 2. For figure legend, see page 1742.

Figure 2 (See previous page). Loss of function of *icd-2* and *icd-1* results in enlarged lysosomes. (**A and B**) NUC-1::mCherry labels tubular and small punctate structures in hypodermal cells in wild-type animals. (**C and D**) NUC-1::mCherry forms big aggregates in the hypodermis in *icd-2(RNAi)* animals. The inserts show magnified views. (**E–H**) Compared with wild-type muscle cells (**E and F**), LAAT-1::GFP-labeled lysosomal structures are much larger in *icd-2(RNAi)* animals (**G and H**). (**I–N**) Compared with coelomocytes in wild-type animals (**I and J**), LMP-1::GFP-labeled lysosomes are much larger in *icd-2(RNAi)* (**K and L**) and *icd-1(RNAi)* (**M and N**) animals. (**A, C, E, G, I, K, and M**): Nomarski images of the animals shown in (**B, D, F, H, J, L, and N**), respectively. (**O–R**) Loss of function of autophagy genes partially suppresses the enlarged lysosome phenotype in coelomocytes in *icd-2(RNAi)* and *icd-1(RNAi)* animals. (**S**) Percentage of LMP-1::GFP-labeled lysosomes with diameters of the indicated size in wild-type, *icd-2(RNAi)* and *icd-1(RNAi)* animals. (**T**) Percentage of lysosomes with diameters of the indicated size in *icd-2, icd-1, icd-2; epg-3, icd-1; epg-3, icd-2; lgg-1* and *lgg-1; icd-1* mutant animals. (**U**) RNAi inactivation of *icd-2* and *icd-1* causes defective degradation of ssGFP in coelomocytes. Young adult animals were used for the heat shock assay. Scale bars: 20 μm (**A–H**), 5 μm (**I–R and U**). Young adult animals were examined in (**A–H**). Animals in (**I–T**) were examined 24 h after the L4 stage.

level of autophagy activity regulates the size of lysosomes in the coelomocytes.[33] Compared with *icd-2* and *icd-1* single mutants, the size of enlarged lysosomes in coelomocytes was reduced in *icd-2; epg-3*, *icd-1; epg-3*, *icd-2; lgg-1*, and *lgg-1; icd-1* double mutants (**Fig. 2O–R and T**), indicating that autophagy activity contributes to the lysosomal abnormality.

We next monitored the degradation of signal sequence-GFP fusion protein (ssGFP), which is driven by a heat shock promoter, to examine lysosome function in coelomocytes. ssGFP is synthesized, secreted into the body cavity and then taken up through endocytosis by coelomocytes, in which it is delivered into lysosomes for degradation.[34] In wild-type animals, ssGFP was almost completely degraded 20 h after heat shock (**Fig. 2U**). In *icd-2(RNAi)* and *icd-1(RNAi)* animals, ssGFP strongly accumulated in the enlarged lysosomes even 48 h after heat shock (**Fig. 2U**), indicating that loss of function of NAC impairs the degradation capability of lysosomes. The enlarged lysosomes in coelomocytes in *icd-2* and *icd-1* mutant animals were still labeled by ASP-1::dsRED and CPR-6::mCherry, which encode lysosome-localized homologs of CTSD (cathepsin D) aspartic protease and a cysteine protease, respectively (**Fig. S3I and S3J**), suggesting that the delivery of lysosome-localized proteases is not generally affected by loss of NAC activity.

ICD-2 and ICD-1 localize on the ER

ICD-2 and ICD-1 contain a NAC domain (**Fig. 3A**). ICD-2 also contains a UBA (ubiquitin-associated) domain at its C terminus (**Fig. 3A**). A transgene expressing mutant ICD-2 with a deletion of the UBA domain rescued the abnormal accumulation of SQST-1 aggregates in *icd-2(tm3125)* mutants (**Fig. S1U and S1V**), indicating that the UBA domain is dispensable for the function of ICD-2 in autophagic degradation of SQST-1.

We performed a yeast 2-hybrid screen to identify ICD-2 interacting proteins. Out of 40 clones, 29 corresponded to ICD-1 (**Fig. S3K**). In an in vitro pulldown assay, GST-fused ICD-2 was specifically pulled down by His-tagged ICD-1 (**Fig. 3B**). By constructing a series of deletion constructs, we found that the interaction between ICD-2 and ICD-1 was mediated by their NAC domains (**Fig. 3B and C**).

ICD-2::GFP and ICD-1::GFP translational fusion reporters were mainly expressed in intestinal cells and muscle cells (**Fig. 3D**). ICD-2 and ICD-1 colocalized with the ER marker TRAM-1::mCherry (**Fig. 3E–G**). Loss of function of ICD-1 dramatically reduced the GFP signal of ICD-2::GFP (**Fig. 3H–K**). Knockdown of ICD-2 also reduced the levels of ICD-1::GFP (**Fig. S3L–S3O**). Thus, formation of the ICD-1 and ICD-2 complex is essential for their stabilities.

Loss of function of *icd-2* and *icd-1* resulted in dramatic upregulation of *Phsp-4::GFP*, a well-characterized ER stress marker (**Fig. 3L–O**; **Fig. S3P and S3Q**), indicating that loss of NAC activity causes ER stress and activates the UPR. The IRE-1-XBP-1 pathway senses ER stress and activates the UPR.[35] Simultaneous depletion of *ire-1* suppressed the upregulation of *Phsp-4::GFP* caused by inactivation of *icd-2* and *icd-1* (**Fig. 3P and Q**; **Fig. S3R and S3S**). However, SQST-1::GFP aggregates still accumulated in *icd-2; ire-1* and *icd-1; ire-1* animals (**Fig. 3R and S**). Therefore, the autophagic defect in *icd-2* and *icd-1* mutants is not due to elevated ER stress.

NAC is required for autophagic flux in mammalian cells

We examined the role of NAC in the autophagy pathway in mammalian cells. The mammalian orthologs of ICD-2 and ICD-1 are encoded by *NACA* and *BTF3*, respectively. In Hela cells, NACA-GFP and BTF3-GFP also colocalized with ER-mCherry (**Fig. S4A–S4F**). Compared with control siRNA-treated cells, siRNA knockdown of *NACA* and *BTF3* led to a significant increase in the number of MAP1LC3 (LC3) puncta, detected by GFP-LC3 or anti-LC3, and also levels of LC3-II, under both nutrient-rich and starvation conditions (**Fig. 4A–H**; **Fig. S4G and S4I–S4K**). NACA-GFP and BTF3-GFP did not form puncta after starvation in HeLa cells.

A block in autophagy flux or elevated autophagy activity could lead to the increased level of LC3-II and number of LC3 puncta. To distinguish these 2 possibilities, *NACA* and *BTF3* knockdown cells were treated with the vacuolar ATPase inhibitor bafilomycin A_1 (BafA1), which blocks autophagosome-lysosome fusion. We found that LC3-II levels and the number of LC3 puncta were not further increased compared with control cells (**Fig. 4H**; **Fig. S4H and S4L**), indicating that loss of NAC activity blocks autophagic flux. We further examined the level of autophagy substrates in *NACA* and *BTF3* knockdown cells. SQSTM1 is a well-characterized autophagy substrate that also mediates the formation and autophagic degradation of ubiquitin-positive protein aggregates. In *NACA* and *BTF3* siRNA-treated cells, SQSTM1 and ubiquitin-positive aggregates dramatically accumulated and colocalized (**Fig. 4I–O**). Levels of SQSTM1 and ubiquitinated proteins were also dramatically increased in an immunoblotting assay (**Fig. 4P and Q**). SQSTM1 and ubiquitin-positive aggregates colocalized with LC3 puncta in *NACA* and *BTF3* knockdown cells (**Fig. S4O–S4W**). Taken together, these results suggest that loss of function of NAC impairs autophagic flux in mammalian cells.

Knockdown of mammalian NAC results in accumulation of nondegradative autolysosomes

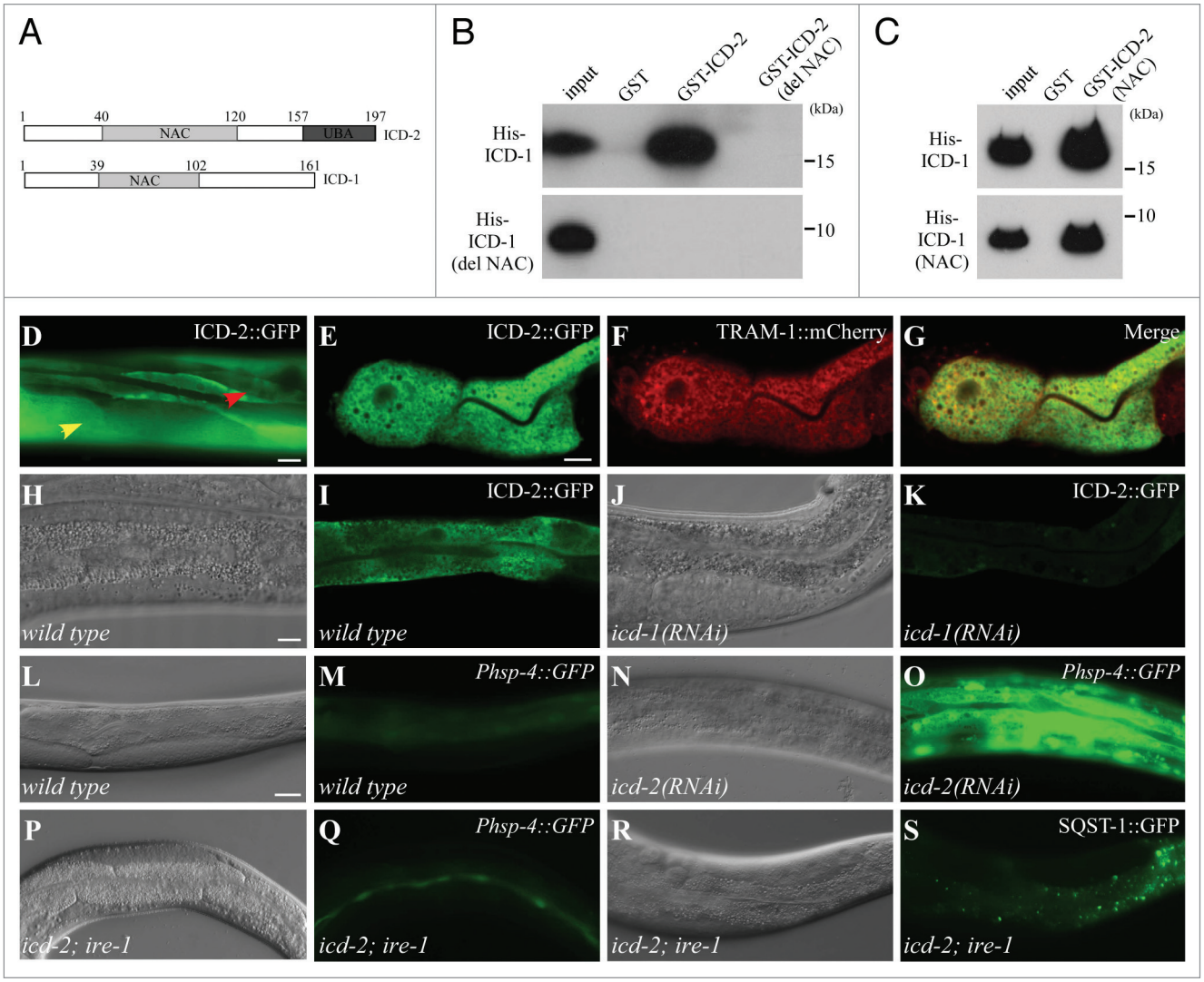

Figure 3. ICD-2 and ICD-1 form a complex and are ER-localized. (**A**) Schematic illustration of the domains in ICD-2 and ICD-1. (**B**) In vitro pulldown assays show that His-tagged ICD-1 pulls down ICD-2, but not a fragment of ICD-2 with a deletion of the NAC domain. Mutant ICD-1 with a deletion of the NAC domain failed to pull down ICD-2. (**C**) The NAC domain mediates the interaction between ICD-2 and ICD-1. (**D**) ICD-2::GFP is expressed in intestinal cells (yellow arrow) and muscle cells (red arrow). (**E–G**) ICD-2::GFP colocalizes with TRAM-1::mCherry-labeled ER in the intestine. (**H–K**) Compared with that in wild-type animals (**H and I**), the expression level of ICD-2::GFP is dramatically decreased in *icd-1(RNAi)* animals (**J and K**). Young adult animals were examined (**D–K**). (**L and M**) *Phsp-4::GFP* is weakly expressed in the intestine in wild-type animals. (**N and O**) Loss of function of *icd-2* dramatically increases the expression of *Phsp-4::GFP*. (**P to S**) Simultaneous loss of *ire-1* activity suppresses the increased expression of *Phsp-4::GFP* (**P and Q**), but not the accumulation of SQST-1::GFP aggregates (**R and S**), in *icd-2(RNAi)* animals. (**H, J, L, N, P, and R**): Nomarski images of the animals shown in (**I, K, M, O, Q, and S**), respectively. Scale bars: 20 μm. L4 larvae were examined (**L–S**).

We next determined at which step the autophagic flux is impaired in NAC knockdown cells. ZFYVE1/DFCP1-labeled omegasomes, which act as cradles for autophagosome formation, exhibited no difference in control and *NACA* and *BTF3* knockdown cells (**Fig. S5A–S5D**). The expression of RFP-GFP-tandemly-tagged LC3 was examined to monitor autophagosome maturation. The GFP fluorescence signal is lost inside acidic and degradative lysosomes, but RFP signal persists. Therefore, the autophagic compartments before fusion with lysosomes are marked by both GFP and RFP, while autolysosomes are labeled only by RFP.[36] Six hours after starvation, only a few autophagosomes labeled by both GFP and RFP or only by RFP were detected in control siRNA-treated cells (**Fig. 5A–C and G**), while in *NACA* and *BTF3* knockdown cells, the number of GFP- and RFP-labeled-autophagosomes and RFP-labeled autolysosomes was dramatically increased (**Fig. 5D–G**). Moreover, $RFP^{+}GFP^{-}$ labeled autolysosomes were enlarged in *NACA* and *BTF3* knockdown cells. Compared with control cells, lysosomes, labeled by LAMP1-Cherry or LysoTracker Red, were dramatically enlarged in *NACA* and *BTF3* knockdown cells (**Fig. S5E–S5K**). Thus, NAC knockdown leads to accumulation of enlarged autolysosomes.

We further investigated the function of autolysosomes in *NACA* and *BTF3* knockdown cells. LC3 puncta, SQSTM1,

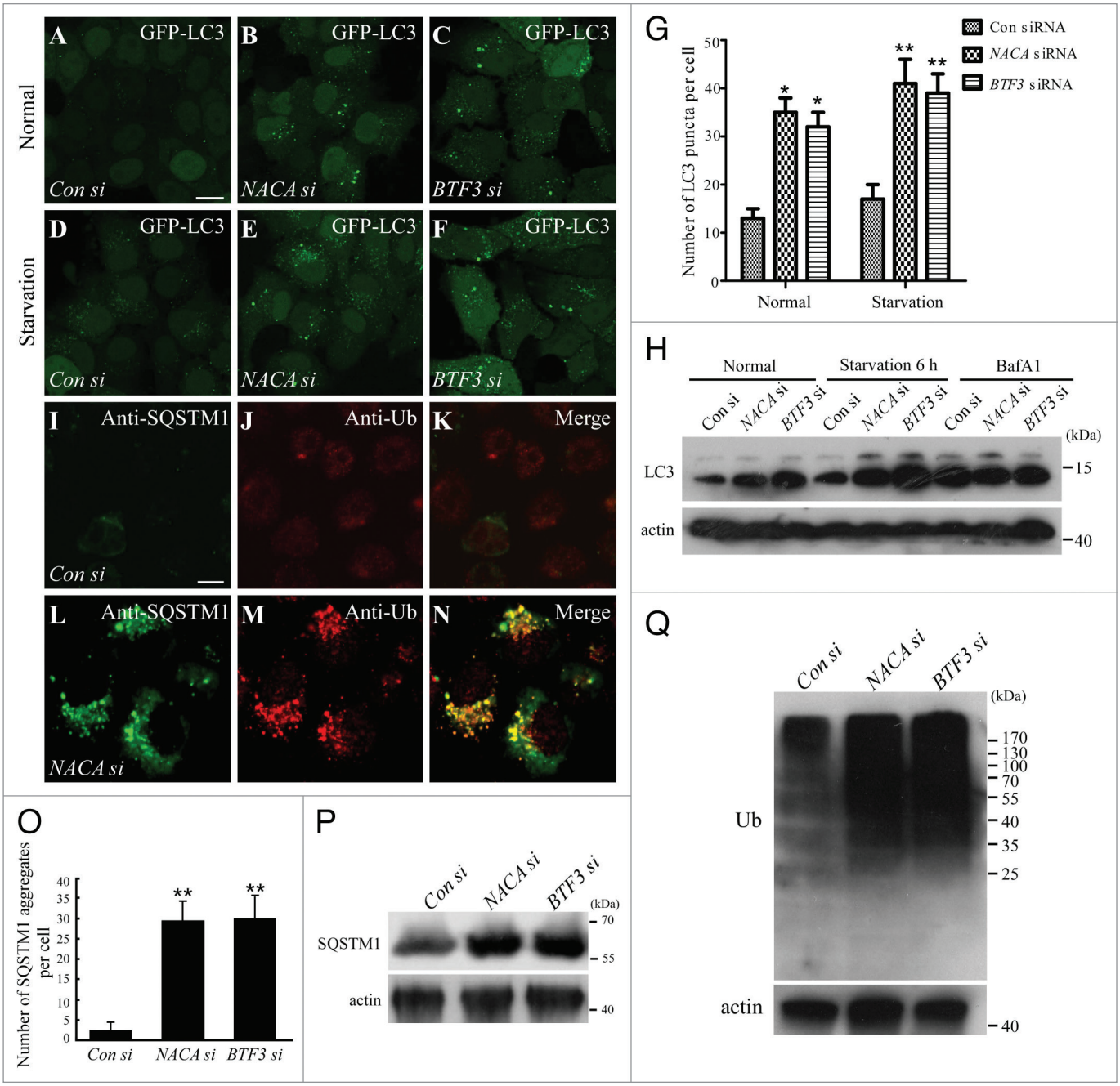

Figure 4. Loss of function of NAC causes a defect in autophagic flux in mammalian cells. (**A–F**) Compared with control (Con) siRNA-treated cells, knockdown of *NACA* and *BTF3* causes accumulation of GFP-LC3 puncta under both normal (**A–C**) and starvation (**D–F**) conditions. (**G**) Number of GFP-LC3 puncta in control, *NACA* and *BTF3* siRNA-treated cells under normal and starvation conditions. *$P < 0.05$, **$P < 0.01$. (**H**) Compared with Con siRNA-treated cells, levels of LC3-II are dramatically increased in *NACA* and *BTF3* knockdown cells under normal and starvation conditions. Knockdown of *NACA* and *BTF3* does not further increase levels of LC3 after BafA1 treatment. (**I–N**) Compared with control cells, SQSTM1 aggregates and Ub-positive aggregates are dramatically increased and colocalize in *NACA* knockdown cells. Scale bars: 10 μm (**A–F and I–N**). (**O**) Number of SQSTM1 aggregates in control, *NACA*, and *BTF3* knockdown cells. ** $P < 0.01$. (**P and Q**) Knockdown of *NACA* and *BTF3* increases levels of SQSTM1 (**P**) and ubiquitinated proteins (**Q**) in immunoblotting assays.

and ubiquitinated protein aggregates accumulated in LAMP1-Cherry- or LysoTracker Red-labeled enlarged lysosomes in *NACA* and *BTF3* knockdown cells after 6 h starvation (**Fig. 5H–O**; **Fig. S5L–S5T**). Knockdown of NAC did not influence processing of CTSB (cathepsin B) or CTSD (**Fig. S5U and S5V**). GFP-LC3 associates with the inner membrane of autophagosomes and is delivered to lysosomes, in which the GFP moiety is cleaved and remains relatively stable, while LC3 is rapidly degraded. Thus, the level of free GFP corresponds to the autophagic rate.[37] Upon starvation, GFP-LC3 was effectively degraded in

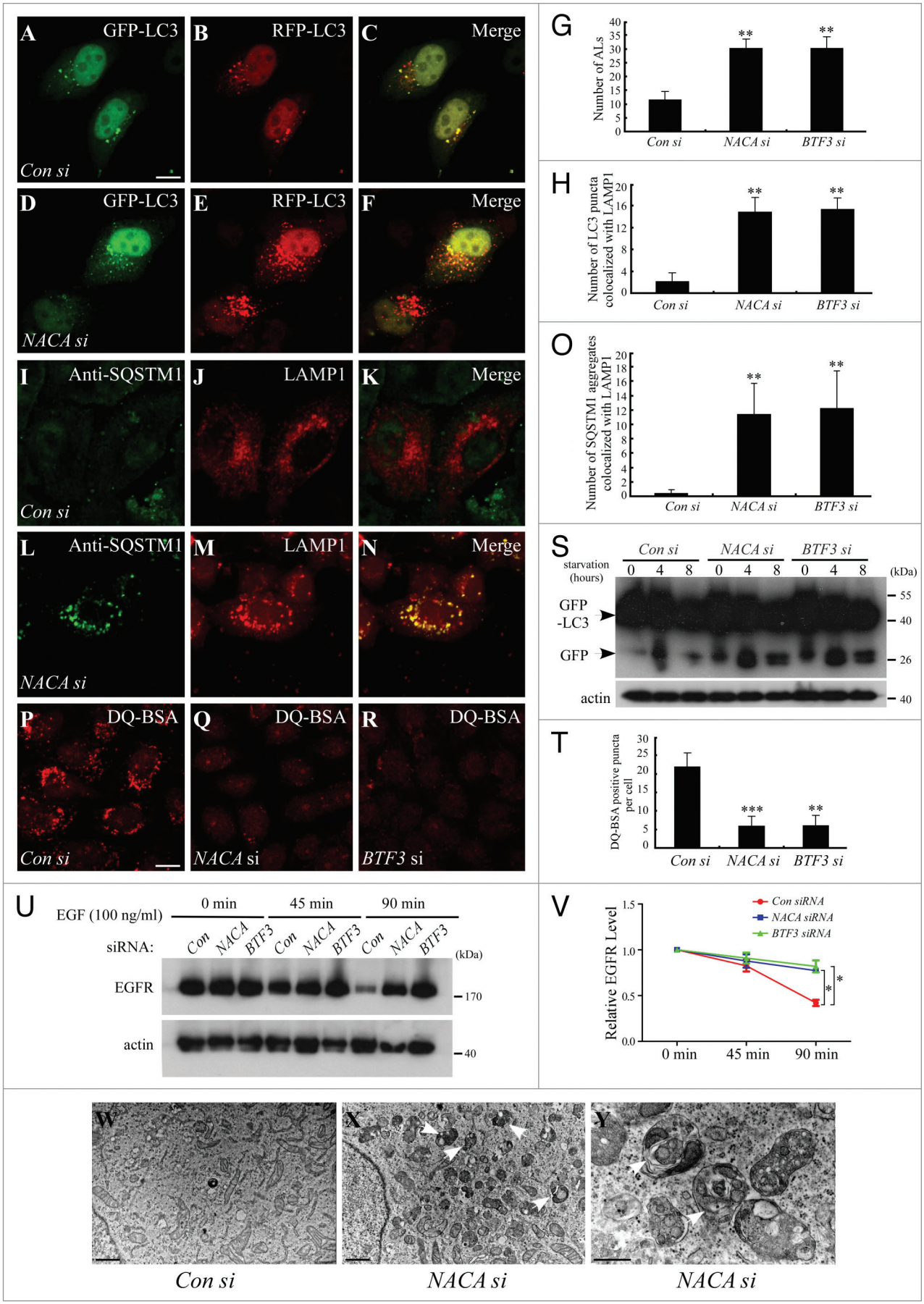

Figure 5 (See previous page). Knockdown of NAC impairs the degradation of autolysosomes. (**A–F**) Compared with control (Con) siRNA-treated cells, knockdown of *NACA* causes accumulation of RFP-LC3-labeled autolysosomes under starvation conditions. (**G**) Number of RFP-positive and GFP-negative LC3-labeled autolysosomes (ALs) in *NACA* and *BTF3* knockdown cells under starvation conditions. $^{**}P < 0.01$. (**H**) Number of LC3 puncta that colocalize with LAMP1-Cherry-labeled lysosomes in control, *NACA,* and *BTF3* knockdown cells. $^{**}P < 0.01$. (**I–N**) Endogenous SQSTM1 aggregates colocalize with LAMP1-Cherry-labeled lysosomes in *NACA* and *BTF3* knockdown cells. (**O**) Number of SQSTM1 aggregates that colocalize with LAMP1 in control, *NACA,* and *BTF3* knockdown cells. Fifty cells were counted. $^{**}P < 0.01$. (**P–R**) Compared with Con siRNA-treated cells, *NACA* and *BTF3* knockdown cells show much less fluorescence signal derived from DQ-BSA degradation. (**S**) Knockdown of *NACA* and *BTF3* causes defective degradation of GFP-LC3. (**T**) Number of DQ-BSA-positive puncta in control, *NACA* and *BTF3* knockdown cells. Fifty cells were counted for each treatment. $^{**}P < 0.01$, $^{***}P < 0.001$. (**U and V**) Compared with Con siRNA-treated cells, EGF-induced EGFR degradation is impaired in *NACA* and *BTF3* knockdown cells. After 90 min, levels of EGFR are dramatically decreased in control cells, but remain high in *NACA* and *BTF3* knockdown cells. Quantification of EGFR levels is shown in (**V**). $^{*}P < 0.05$. (**W–Y**) Knockdown of *NACA* causes accumulation of autolysosomes (arrows). Scale bars: 10 μm (**A–F, I–N, and P–R**), 1 μm (**W and X**), 500 nm (**Y**).

NS siRNA-treated cells. Levels of free GFP were high at 4 h after starvation, but dramatically reduced 8 h after starvation. However, levels of free GFP accumulated in both *NACA* and *BTF3* knockdown cells even 8 h after starvation (**Fig. 5S**). The degradative capacity of autolysosomes can also be monitored by examining the fluorescence signal derived from lysosomal degradation of DQ-BSA, a bovine serum albumin derivative conjugated to a self-quenched fluorophore.[38] Compared with NS siRNA-treated cells, the fluorescence signal was much lower in *NACA* and *BTF3* knockdown cells (**Fig. 5P–T**). We also measured levels of epidermal growth factor receptor (EGFR), which is internalized from the cell surface upon ligand activation, sorted into late endosomes and degraded in lysosomes. After EGF treatment, the EGFR level gradually decreased in control cells, while degradation of EGFR was significantly reduced in *NACA* and *BTF3* knockdown cells (**Fig. 5U and V**).

Finally, we performed TEM to examine the ultra-structure of autophagic structures in NAC knockdown cells. In NS siRNA-treated HeLa cells, autolysosomes were barely detected 6 h after starvation. However, *NACA* and *BTF3* siRNA-treated cells showed accumulation of a large number of late autophagic elements, including amphisomes and autolysosomes (**Fig. 5W–Y**). Many abnormal autolysosomes had electron-dense contents in *NACA* and *BTF3* knockdown cells (**Fig. 5Y** and data not shown). Taken together, these results show that degradation by lysosomes is greatly impaired and nondegradative autolysosomes accumulate in *NACA* and *BTF3* knockdown cells.

Discussion

Here we showed that NAC is required for autophagic flux in *C. elegans* and also in mammalian cells. Loss of function of NAC causes the accumulation of enlarged lysosomes and greatly impairs the degradation function of lysosomes. How does loss of function of NAC impair the function of lysosomes? NAC protects emerging polypeptides from interaction with other cytoplasmic proteins to ensure appropriate cotranslational targeting of nascent proteins to the ER and mitochondria.[1] In *C. elegans*, loss of NAC induces the expression of markers for ER stress and mitochondrial stress (data not shown), consistent with the function of NAC in preventing inappropriate localization of proteins to the ER and mitochondria.[11] Loss of function of NAC could cause mistargeting of proteins into the ER that are essential for the function of lysosomes. NAC may also function in targeting proteins directly into lysosomes. Lysosomal enzymes, including ASP-1 and CPR-6 in *C. elegans* and CTSB and CTSD in mammalian cells, are not affected after NAC knockdown, indicating that lysosomal proteases are not generally mislocalized. NAC also acts as a translational chaperone, assisting proper protein folding and also protecting emerging nascent chains from proteolysis.[7,8] Loss of function of NAC may cause accumulation of misfolded proteins and enhance protein aggregation, which subsequently congests the lysosome and impairs its function. Alternatively, NAC may impair the endocytic trafficking pathway, which in turn affects autophagosome maturation. Consistent with this, loss of NAC activity in *C. elegans* causes accumulation of vacuoles originating from endosomes.

During *C. elegans* embryogenesis, loss of *icd-1* activity causes a marked increase in apoptosis, with neurons more sensitive to removal of ICD-1 than other cell types.[10] Mutations in autophagy genes involved in autophagosome formation do not increase the frequency of cell death during embryogenesis but cause a slower removal of apoptotic cell corpses.[39,40] Thus, inappropriate cell death may be specific to NAC loss-of-function mutants, in which the lysosomes are enlarged and nondegradative. Accumulation of nondegradative autolysosomes containing aggregate-prone disease-related proteins has been shown in a variety of neurodegenerative diseases, and may cause neuronal death.[41] NAC has been shown to maintain protein homeostasis by linking translational activity to protein-folding status in *C. elegans*.[12] NAC associates with ribosomes to promote translation and assist protein folding under nonstress conditions. During proteotoxic stress conditions such as aging and heat shock, in which misfolded and aggregated proteins accumulate, NAC disassociates from the ribosome and redistributes to protein aggregates, resulting in reduced translational capacity.[12] Our study reveals that NAC plays an essential role in the autophagic degradation of protein aggregates, providing a mechanistic insight into how NAC balances proteostasis under physiological conditions.

Methods and Materials

Strains

The following strains were used in this work: *bpIs151(Psqst-1::sqst-1::GFP, unc-76(+))*, *icd-2(tm3125)*, *icd-1(tm2873)*, *atg-3(bp412)*, *yqIs25(Plgg-1::GFP::LGG-1)*, *pwIs50 (Plmp-1::LMP-1::GFP)*, *qxIs354(Pced-1:-LAAT-1::GFP)*, *zcIs4(Phsp-4::GFP)*, *arIs36(Phsp::ssGFP)*, *qxIs300(Plgg-1::mCherry::LGG-1)* and

qxIs257(Pced-1::NUC-1::mCherry). *tm3125* deletes 433 bp covering exons 2 and 3 of *icd-2*. *tm2873* deletes 243 bp covering the promoter and exon 1 of *icd-1*.

RNAi injection

For RNAi injection experiments, single-stranded RNA was transcribed from T7- and SP6-flanked PCR templates. ssRNAs were then annealed and injected into animals carrying various reporters. F1 progeny were examined for the corresponding phenotype.

Reporter construction

ICD-2::GFP and *ICD-1::GFP* reporters were constructed by cloning the corresponding coding sequence into pPD95.79 with in-frame fusion with GFP. The constructs were coinjected with pRF4(*rol-6(su1006)*) into wild-type animals.

Cell culture

HeLa cells were cultured in DMEM (Hyclone, SH30022.01B) with 10% fetal bovine serum (FBS) (Hyclone, SH30084.03) supplemented with 50 μg/mL penicillin-streptomycin solution. All cells were maintained at 37 °C in a humidified atmosphere with 5% CO2. For starvation assays, cells were washed 3 times with phosphate-buffered saline (PBS; 137 mM NaCl, 2.7 mM KCl, 10 mM Na_2HPO_4, 2 mM KH_2PO_4, PH 7.4) and incubated in DMEM (Hyclone, SH30022.01B) without FBS (Hyclone, SH30084.03) for 2 h at 37 °C. For BafA1 (Sigma, B1793) treatment, cells were cultured in DMEM (Hyclone, SH30022.01B) containing 10% FBS (Hyclone, SH30084.03) and BafA1 (20 nM) for 4 h. For LysoTracker Red staining, 100 nM LysoTracker Red (Invitrogen, L7528) was added into culture medium for 30 min before analysis.

siRNA and plasmid transfection

NACA siRNAs, *BTF3* siRNAs, and nonsense control siRNAs were purchased from GenePharma. Cells were transfected with siRNAs or mock-transfected using Lipofectamine RNAi MAX (Invitrogen, 13778150) for 72 h according to the manufacturer's instructions. Plasmid transfection was performed using Lipofectamine 2000 (Invitrogen, 11668019) for 24 h. Cells were then harvested for immunofluorescence staining or immunoblotting. The siRNA sequences used in this study are:

non-sense, 5'-UUCUCCGAAC GUGUCACGUT T-3';

NACA, 5'-GCGAUUAUGG AAUUAACAA-3';

BTF3, 5'-GAAGUUCCAG AUCUUGUGG-3'.

Immunofluorescence staining

Cells grown on coverslips were washed with PBS 3 times, fixed with 4% paraformaldehyde in PBS for 10 min at room temperature and subsequently treated with ice-cold methanol at -20 °C for 5 min. Cells were blocked with goat serum (ZSGB-BIO, ZLI9056) for one h at room temperature, and were then incubated with primary antibodies diluted in goat serum overnight. After at least 3 PBS washes, cells were incubated with secondary antibodies diluted in goat serum for one h. Cells were then washed with PBS and the coverslips were mounted on microscope slides with mounting medium with DAPI (Vector Laboratories, H-1200). The fluorescence was checked with a confocal microscope (LSM710, Carl Zeiss, Jena, Germany). The following antibodies were used in this study: LC3B (Cell Signaling Technology, 2775s), mouse anti-SQSTM1/p62 (MBL, PM045), anti-ubiquitin (Cell Signaling Technology, 3936s), CTSD/cathepsin D (Abcam, ab75852), CTSB/cathepsin B (Abcam, ab58802).

Immunoblotting assay

For immunoblotting assays in *C. elegans,* lysates were prepared from 200 worms and proteins were detected with diluted primary antibody and HRP-conjugated anti-rabbit secondary antibody (Sigma, A0545) or anti-mouse secondary antibody (Sigma, A9044). As a gel loading control, anti-actin monoclonal antibody (Sigma, A3853) was used.

For immunoblotting assays in mammalian cells, cells were washed with PBS (137 mM NaCl, 2.7 mM KCl, 10 mM Na2HPO4, 2 mM KH2PO4; pH 7.4) 3 times and harvested in lysis buffer (ThermoFisher, 78501) supplemented with protease inhibitor cocktail (Roche, 11836170001). Cell lysates were centrifuged for 15 min at 4 °C at 15, 000 g. The supernatant fraction was subjected to SDS-PAGE and proteins were detected using corresponding primary and secondary antibodies.

DQ-BSA degradation assay

Cells were serum starved for 2 h and then incubated with 10 μg/ml DQ-BSA (Life Technologies, P12051) for 30 min. Cells were washed with PBS, fixed, and then examined by a confocal microscope (LSM 710, Carl Zeiss, Jena, Germany).

EGFR degradation assay

Cells were serum-starved for 16 h and then treated with 100 ng/ml EGF (Life Technologies, PMG8043) and 25 μg/ml cycloheximide (Sigma, N11534) for the indicated time. Cells were then washed with PBS and lysed with cell lysis buffer (ThermoFisher, 78501). Degradation of EGFR was examined using an immunoblotting assay with the anti-EGFR antibody (Santa Cruz Biotechnology, sc-03).

Electron microscopy (EM)

To prepare ultrathin cell sections for EM, control, *NACA* and *BTF3* knockdown HeLa cells were starved for 2h. Samples were then fixed with 2.5% glutaraldehyde in PBS for 2 h at room temperature followed by 1.5 h in 2% OsO_4 and were then dehydrated by an ethanol series. Embedded samples were sectioned (70 nm) and placed on formvar, carbon-coated copper grids (Polysciences, 24924). Grids were stained with uranyl acetate and lead citrate. Samples were examined using a 120 kV Jeol electron microscope (JEM-1400, Germany) at 80 kV. Images were photographed by a Gatan-832 digital camera (SC1000, Gatan, USA).

Statistical analysis

Data from at least 3 sets of samples were used for statistical analysis. Statistical significance was calculated by the Student *t* test. $P < 0.05$ was considered significant.

Disclosure of Potential Conflicts of Interest

No potential conflicts of interest were disclosed.

Acknowledgments

We thank Dr Isabel Hanson for critical appraisal of the manuscript. This work was supported by the National Basic Research Program of China (2013CB910100, 2011CB910100) to HZ. The research of Hong Zhang was supported in part by

an International Early Career Scientist grant from the Howard Hughes Medical Institute.

Supplemental Materials

Supplemental materials may be found here:
www.landesbioscience.com/journals/autophagy/article/29638

References

1. Rospert S, Dubaquié Y, Gautschi M. Nascent-polypeptide-associated complex. Cell Mol Life Sci 2002; 59:1632-9; PMID:12475173; http://dx.doi.org/10.1007/PL00012490
2. Wiedmann B, Sakai H, Davis TA, Wiedmann M. A protein complex required for signal-sequence-specific sorting and translocation. Nature 1994; 370:434-40; PMID:8047162; http://dx.doi.org/10.1038/370434a0
3. Wang S, Sakai H, Wiedmann M. NAC covers ribosome-associated nascent chains thereby forming a protective environment for regions of nascent chains just emerging from the peptidyl transferase center. J Cell Biol 1995; 130:519-28; PMID:7622554; http://dx.doi.org/10.1083/jcb.130.3.519
4. Zhang Y, Berndt U, Gölz H, Tais A, Oellerer S, Wölfle T, Fitzke E, Rospert S. NAC functions as a modulator of SRP during the early steps of protein targeting to the endoplasmic reticulum. Mol Biol Cell 2012; 23:3027-40; PMID:22740632; http://dx.doi.org/10.1091/mbc.E12-02-0112
5. Fünfschilling U, Rospert S. Nascent polypeptide-associated complex stimulates protein import into yeast mitochondria. Mol Biol Cell 1999; 10:3289-99; PMID:10512867; http://dx.doi.org/10.1091/mbc.10.10.3289
6. George R, Walsh P, Beddoe T, Lithgow T. The nascent polypeptide-associated complex (NAC) promotes interaction of ribosomes with the mitochondrial surface in vivo. FEBS Lett 2002; 516:213-6; PMID:11959135; http://dx.doi.org/10.1016/S0014-5793(02)02528-0
7. Koplin A, Preissler S, Ilina Y, Koch M, Scior A, Erhardt M, Deuerling E. A dual function for chaperones SSB-RAC and the NAC nascent polypeptide-associated complex on ribosomes. J Cell Biol 2010; 189:57-68; PMID:20368618; http://dx.doi.org/10.1083/jcb.200910074
8. del Alamo M, Hogan DJ, Pechmann S, Albanese V, Brown PO, Frydman J. Defining the specificity of cotranslationally acting chaperones by systematic analysis of mRNAs associated with ribosome-nascent chain complexes. PLoS Biol 2011; 9:e1001100; PMID:21765803; http://dx.doi.org/10.1371/journal.pbio.1001100
9. Markesich DC, Gajewski KM, Nazimiec ME, Beckingham K. bicaudal encodes the *Drosophila* beta NAC homolog, a component of the ribosomal translational machinery. Development 2000; 127:559-72; PMID:10631177
10. Bloss TA, Witze ES, Rothman JH. Suppression of CED-3-independent apoptosis by mitochondrial betaNAC in *Caenorhabditis elegans.* Nature 2003; 424:1066-71; PMID:12944970; http://dx.doi.org/10.1038/nature01920
11. Arsenovic PT, Maldonado AT, Colleluori VD, Bloss TA. Depletion of the *C. elegans* NAC engages the unfolded protein response, resulting in increased chaperone expression and apoptosis. PLoS One 2012; 7:e44038; PMID:22957041; http://dx.doi.org/10.1371/journal.pone.0044038
12. Kirstein-Miles J, Scior A, Deuerling E, Morimoto RI. The nascent polypeptide-associated complex is a key regulator of proteostasis. EMBO J 2013; 32:1451-68; PMID:23604074; http://dx.doi.org/10.1038/emboj.2013.87
13. Nakatogawa H, Suzuki K, Kamada Y, Ohsumi Y. Dynamics and diversity in autophagy mechanisms: lessons from yeast. Nat Rev Mol Cell Biol 2009; 10:458-67; PMID:19491929; http://dx.doi.org/10.1038/nrm2708
14. Xie Z, Klionsky DJ. Autophagosome formation: core machinery and adaptations. Nat Cell Biol 2007; 9:1102-9; PMID:17909521; http://dx.doi.org/10.1038/ncb1007-1102
15. Longatti A, Tooze SA. Vesicular trafficking and autophagosome formation. Cell Death Differ 2009; 16:956-65; PMID:19373247; http://dx.doi.org/10.1038/cdd.2009.39
16. Razi M, Chan EY, Tooze SA. Early endosomes and endosomal coatomer are required for autophagy. J Cell Biol 2009; 185:305-21; PMID:19364919; http://dx.doi.org/10.1083/jcb.200810098
17. Filimonenko M, Stuffers S, Raiborg C, Yamamoto A, Malerød L, Fisher EM, Isaacs A, Brech A, Stenmark H, Simonsen A. Functional multivesicular bodies are required for autophagic clearance of protein aggregates associated with neurodegenerative disease. J Cell Biol 2007; 179:485-500; PMID:17984323; http://dx.doi.org/10.1083/jcb.200702115
18. Zhang Y, Yan L, Zhou Z, Yang P, Tian E, Zhang K, Zhao Y, Li Z, Song B, Han J, et al. SEPA-1 mediates the specific recognition and degradation of P granule components by autophagy in *C. elegans.* Cell 2009; 136:308-21; PMID:19167332; http://dx.doi.org/10.1016/j.cell.2008.12.022
19. Tian Y, Li Z, Hu W, Ren H, Tian E, Zhao Y, Lu Q, Huang X, Yang P, Li X, et al. *C. elegans* screen identifies autophagy genes specific to multicellular organisms. Cell 2010; 141:1042-55; PMID:20550938; http://dx.doi.org/10.1016/j.cell.2010.04.034
20. Lu Q, Wu F, Zhang H. Aggrephagy: lessons from *C. elegans.* Biochem J 2013; 452:381-90; PMID:23725457; http://dx.doi.org/10.1042/BJ20121721
21. Tian E, Wang F, Han J, Zhang H. *epg-1* functions in autophagy-regulated processes and may encode a highly divergent Atg13 homolog in *C. elegans.* Autophagy 2009; 5:608-15; PMID:19377305; http://dx.doi.org/10.4161/auto.5.5.8624
22. Yang P, Zhang H. The coiled-coil domain protein EPG-8 plays an essential role in the autophagy pathway in *C. elegans.* Autophagy 2011; 7:159-65; PMID:21116129; http://dx.doi.org/10.4161/auto.7.2.14223
23. Lu Q, Yang P, Huang X, Hu W, Guo B, Wu F, Lin L, Kovács AL, Yu L, Zhang H. The WD40 repeat PtdIns(3)P-binding protein EPG-6 regulates progression of omegasomes to autophagosomes. Dev Cell 2011; 21:343-57; PMID:21802374; http://dx.doi.org/10.1016/j.devcel.2011.06.024
24. Liang Q, Yang P, Tian E, Han J, Zhang H. The *C. elegans* ATG101 homolog EPG-9 directly interacts with EPG-1/Atg13 and is essential for autophagy. Autophagy 2012; 8:1426-33; PMID:22885670; http://dx.doi.org/10.4161/auto.21163
25. Yang P, Zhang H. You are what you eat: multifaceted functions of autophagy during *C. elegans* development. Cell Res 2014; 24:80-91; PMID:24296782; http://dx.doi.org/10.1038/cr.2013.154
26. Gutierrez MG, Munafó DB, Berón W, Colombo MI. Rab7 is required for the normal progression of the autophagic pathway in mammalian cells. J Cell Sci 2004; 117:2687-97; PMID:15138286; http://dx.doi.org/10.1242/jcs.01114
27. Jäger S, Bucci C, Tanida I, Ueno T, Kominami E, Saftig P, Eskelinen EL. Role for Rab7 in maturation of late autophagic vacuoles. J Cell Sci 2004; 117:4837-48; PMID:15340014; http://dx.doi.org/10.1242/jcs.01370
28. Ju JS, Fuentealba RA, Miller SE, Jackson E, Piwnica-Worms D, Baloh RH, Weihl CC. Valosin-containing protein (VCP) is required for autophagy and is disrupted in VCP disease. J Cell Biol 2009; 187:875-88; PMID:20008565; http://dx.doi.org/10.1083/jcb.200908115
29. Tresse E, Salomons FA, Vesa J, Bott LC, Kimonis V, Yao TP, Dantuma NP, Taylor JP. VCP/p97 is essential for maturation of ubiquitin-containing autophagosomes and this function is impaired by mutations that cause IBMPFD. Autophagy 2010; 6:217-27; PMID:20104022; http://dx.doi.org/10.4161/auto.6.2.11014
30. Nazarko TY, Huang J, Nicaud JM, Klionsky DJ, Sibirny AA. Trs85 is required for macroautophagy, pexophagy and cytoplasm to vacuole targeting in Yarrowia lipolytica and Saccharomyces cerevisiae. Autophagy 2005; 1:37-45; PMID:16874038; http://dx.doi.org/10.4161/auto.1.1.1512
31. Bánréti Á, Lukácsovich T, Csikós G, Erdélyi M, Sass M. PP2A regulates autophagy in two alternative ways in *Drosophila.* Autophagy 2012; 8:623-36; PMID:22330894; http://dx.doi.org/10.4161/auto.19081
32. Liu B, Du H, Rutkowski R, Gartner A, Wang X. LAAT-1 is the lysosomal lysine/arginine transporter that maintains amino acid homeostasis. Science 2012; 337:351-4; PMID:22822152; http://dx.doi.org/10.1126/science.1220281
33. Sun T, Wang X, Lu Q, Ren H, Zhang H. CUP-5, the *C. elegans* ortholog of the mammalian lysosomal channel protein MLN1/TRPML1, is required for proteolytic degradation in autolysosomes. Autophagy 2011; 7:1308-15; PMID:21997367; http://dx.doi.org/10.4161/auto.7.11.17759
34. Grant BD, Sato M. Intracellular trafficking. WormBook 2006; •••:1-9; PMID:18050485
35. Cao SS, Kaufman RJ. Unfolded protein response. Curr Biol 2012; 22:R622-6; PMID:22917505; http://dx.doi.org/10.1016/j.cub.2012.07.004
36. Kimura S, Noda T, Yoshimori T. Dissection of the autophagosome maturation process by a novel reporter protein, tandem fluorescent-tagged LC3. Autophagy 2007; 3:452-60; PMID:17534139; http://dx.doi.org/10.4161/auto.4451
37. Mizushima N, Yoshimori T, Levine B. Methods in mammalian autophagy research. Cell 2010; 140:313-26; PMID:20144757; http://dx.doi.org/10.1016/j.cell.2010.01.028
38. Vázquez CL, Colombo MI. Assays to assess autophagy induction and fusion of autophagic vacuoles with a degradative compartment, using monodansylcadaverine (MDC) and DQ-BSA. Methods Enzymol 2009; 452:85-95; PMID:19200877; http://dx.doi.org/10.1016/S0076-6879(08)03606-9
39. Huang S, Jia K, Wang Y, Zhou Z, Levine B. Autophagy genes function in apoptotic cell corpse clearance during *C. elegans* embryonic development. Autophagy 2013; 9:138-49; PMID:23108454; http://dx.doi.org/10.4161/auto.22352
40. Cheng S, Wu Y, Lu Q, Yan J, Zhang H, Wang X. Autophagy genes coordinate with the class II PI/PtdIns 3-kinase PIKI-1 to regulate apoptotic cell clearance in *C. elegans.* Autophagy 2013; 9:2022-32; PMID:24165672; http://dx.doi.org/10.4161/auto.26323
41. Nixon RA, Yang DS, Lee JH. Neurodegenerative lysosomal disorders: a continuum from development to late age. Autophagy 2008; 4:590-9; PMID:18497567; http://dx.doi.org/10.4161/auto.6259